NUMERICAL SIMULATION OF HEAT AND MASS TRANSFER IN A 2D LID-DRIVEN CAVITY

Leonardo Carvalho de Jesus, leonardocjes@gmail.com
Julio Tomás Aquije Chacaltana, juliotac@gmail.com
LABESUL, Universidade Federal do Espírito Santo. Av. Fernando Ferrari, 514, Goiabeiras, Vitória – ES.

Abstract. *The steady state of combined thermal and mass transport by convection-diffusion in a square lid-driven cavity is studied. The fluid flow is solved by using the vorticity-stream function formulation and transport of temperature and mass are solved by an advection-diffusion equation. The set of governing equations are solved numerically by a second-order finite difference scheme in time and space in a regular grid. The flow, heat and mass transfer are examined in the domain of the Reynolds (Re), Schimidt (Sc), Richardson (Ri), Lewis (Le) dimensionless numbers and the buoyancy ratio parameter (N), covering a wide range of applications. Results shown that Grasolf and Reynolds numbers play an important role in the mass and energy transport either enhancing or retarding this process and the intensification of heat transfer occur when $Gr/Re \ll 1$. Comparisons with former investigations are performed and the results shown good agreement.*

Keywords*: Lid-driven cavity, mixed convection, numerical simulation*

1. NOMENCLATURE

Symbols	
G_{rS}	Solutal Grasolf number ($g\beta_C(C_{hot} - C_{cold})H^3/\nu^2$)
G_{rT}	Thermal Grasolf number ($g\beta_T(T_{hot} - T_{cold})H^3/\nu^2$)
U_0	Dimensionless lid velocity (−)
$\vec{n}$	Unit normal vector (−)
s	Unit tangential vector (−)
Δt	Model time step (s)
$\Delta x, \Delta y$	Grid size in x and y directions (m)
C	Mass concentration ($kg\ m^{-3}$)
D	Mass diffusivity ($m^2 s^{-1}$)
H	Cavity height (m)
L	Cavity length (m)
N	Buoyant ratio number (G_{rS}/G_{rT})
P	Dimensionless pressure (−)
Pr	Prandtl number (ν/κ)
Re	Reynolds number ($U_0 H/\nu$)
Ri	Richardson number (G_{rT}/Re^2)
Sc	Schmidt number (D/κ)
T	Temperature ($°C$)
U, V	Dimensionless velocity components (−)
X, Y	Dimensionless coordinates (−)
g	Gravitational acceleration (ms^{-2})
nx, ny	Number of grid point in the x and y axis
t	Time (s)
u, v	Velocity components in x and y axis (ms^{-1})
x, y	Cartesian coordinates (m)
$\boldsymbol{V}$	Dimensionless velocity vector (−)

Greek symbols	
β_C	Volumetric solutal expansion coefficient ($m^3\ kg$)
β_T	Volumetric thermal expansion coefficient ($°C^{-1}$)
ρ_0	Characteristic density ($kg\ m^{-3}$)
Φ	Dimensionless mass concentration (−)
Ψ	Dimensionless stream function (−)
Ω	Dimensionless vorticity (−)
β	Relaxation parameter (−)
θ	Dimensionless temperature (−)
κ	Thermal diffusivity ($m^2 s^{-1}$)
ν	Dynamic viscosity ($m^2 s^{-1}$)
ρ	Density ($kg\ m^{-3}$)
τ	Dimensionless time (−)
ψ	Stream function ($m^2 s$)
ω	Vorticity (s^{-1})

Subscripts	
i, j	Mesh indices in the y and x axis
$cold$	Cold wall
hot	Hot wall

Superscripts	
k	Iteration index
n	Time index

2. INTRODUCTION

The lid-driven cavity is one of the simplest benchmarks to validate numerical codes and study dynamics and transport phenomena for several flow and fluid conditions. The mass and heat transport governs many process in nature as well as in engineering applications, such as spray and flash drying, combustion of atomized liquid fuels, crystal growth, material and separation process, cyclone evaporation, ocean currents and eddy dynamics, etc (Lee et al., 1988; Al-Amiri et al.,

2007) in which its understanding require the knowledge of dynamics resulting from the free and forced convection and buoyant forces due to thermal and mass transport and also the resulting hydrodynamics.

Several research have been reported in literature in flow dynamics of the lid-driven flow in a large range of Reynold numbers (e.g Ghia et al, 1982; Botella and Peyret, 1998; Erturk and Gökçöl, 2006; Bruneau and Saad, 2006) and in the natural and forced convection due to buoyant forces. For example Mahamed predicted the flow and mass transport in a shallow, lid-driven cavity for low Prandtl numbers, considering heating in either top and bottom walls; while Ben presented experimental and numerical results for the mixed heat transfer un a shallow cavity with a sliding bottom wall. Aydin simulated the mass transport mechanism for laminar mixed convection for a buoyant and shear driven cavity. Recently, Al-Amiri et al. (2006) studied with a finite-element numerical model the mixed convection combining both buoyant forces arising from both thermal and diffusion. They studied the flow, mass and heat transport for a wide range of dimensionless operational parameters (Richardson, Lewis, Reynolds numbers and buoyant ratio parameter) and gave insights of effects of the buoyant forces and high transport phenomena.

In this paper we studied both flow and transport phenomena in a bottom heated 2D lid-driven with adiabatic side walls. We numerically solved the streamfunction-vorticity and transport equations with a second order finite-difference in both time and space domains. The buoyant ratio number, Lewis, and Richardson numbers were utilized to explore the transport of both mass and heat in a broad range of values

3. METHODOLOGY

3.1 Mathematical model

We studied the flow, mass and heat transport in a two-dimensional cavity of height H and length L filled with an incompressible Newtonian mixture of a binary fluid in a laminar regime. Vertical walls are considered to be adiabatic and impermeable, the bottom wall has temperature T_{hot} and concentration C_{hot}, while top wall has T_{cold} and C_{cold} temperature and concentration, respectively ($T_{hot} > T_{cold}$ and $C_{hot} > C_{cold}$). The sketch of the physical problem is shown in the Fig. 1.

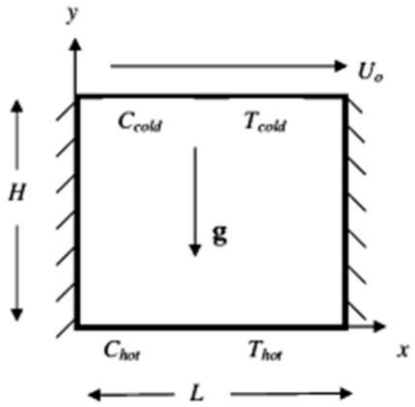

Figure 1- Sketch of the physical cavity and coordinates. Source: Al-Amiri et al. (2007).

Both top and bottom walls can be considered with infinite mass and heat diffusivities. Moreover, the top wall slides from left to right with a constant velocity U_0. The fluid density is assumed to vary with both temperature and concentrations given by the relation $\rho = \rho_0\left[1 - \beta_T(T - T_{cold}) - \beta_C(C - C_{cold})\right]$, where ρ_0 is the characteristic density, β_T and β_C are the volumetric expansion coefficients due to temperature and mass, respectively. In this work, we followed methodology from Al-Amiri et al. (2007) and assumed that β_T can assume only positive values, while β_C can be either positive or negative for cooperative or opposing flows, respectively. The set of equations that governs the flow and mass and heat transport are adimensionalized following the dimensionless variables (Eq. 1):

$$X = \frac{x}{H}; \quad Y = \frac{y}{H}; \quad \tau = \frac{tU_0}{H}; \quad \theta = \frac{T - T_{cold}}{T_{hot} - T_{cold}}; \quad \Phi = \frac{C - C_{cold}}{C_{hot} - C_{cold}} \tag{1}$$

Where x and y are the Cartesian coordinates along the length and the height of the cavity, respectively; T is the fluid temperature, C the fluid concentration and t is the time. The X and Y, τ, θ and Φ are the dimensionless space coordinates, time, temperature and mass, respectively. The dimensionless governing equations for the fluid flow are shown in Eq. 2 and Eq. 3, while temperature and mass dimensionless advection-diffusion are shown in Eq. 4 and Eq. 5, respectively.

$$\nabla . \boldsymbol{V} = 0 \tag{2}$$

$$\frac{\partial \boldsymbol{V}}{\partial \tau} + (\boldsymbol{V}.\nabla)\boldsymbol{V} = \frac{1}{Re}\nabla^2 \boldsymbol{V} + \frac{G_{rT}}{Re^2}\left(\theta + \frac{G_{r,S}}{G_{rT}}\boldsymbol{\Phi}\right) - \nabla P \tag{3}$$

$$\frac{\partial \theta}{\partial \tau} + \boldsymbol{V}.\nabla\theta = \frac{1}{PrRe}\nabla^2\theta \tag{4}$$

$$\frac{\partial \boldsymbol{\Phi}}{\partial \tau} + \boldsymbol{V}.\nabla\boldsymbol{\Phi} = \frac{1}{ScRe}\nabla^2\boldsymbol{\Phi} \tag{5}$$

Where $\boldsymbol{V}$ is the velocity vector, P is the dimensioless pressure, $Re = U_0 H/\nu$ is the Reynolds number, $Sc = \nu/D$ is the Schmidt number, $Pr = \nu/\kappa$ is the Prandtl number; $G_{rT} = g\beta_T(T_{hot} - T_{cold})H^3/\nu^2$ and $G_{r,S} = g\beta_C(C_{hot} - C_{cold})H^3/\nu^2$ are the thermal and solutal Grasolf numbers, respectively. Also g is the gravity acceleration, ν the dynamic viscosity and D and κ the mass and thermal diffusivities.

The set of *momentum* and transport equations are solved using the stream function and vorticity variables leading to a system of elliptic-parabolic equations. The stream function/vorticity formulation can be represented as:

$$U = \frac{\partial \Psi}{\partial y};\quad V = -\frac{\partial \Psi}{\partial x},\qquad \Omega = \frac{\partial V}{\partial X} - \frac{\partial U}{\partial Y} \tag{6}$$

From mass conservation of an incompressible fluid, we can deduce that:

$$\Omega = -\nabla^2 \Psi \tag{7}$$

Substituting the Eq. 6 in the Eq.'s 3-5 we obtain three scalar equations to solve the time evolution of vorticity, temperature and mass, given by:

$$\frac{\partial \Omega}{\partial \tau} + \left(U\frac{\partial \Omega}{\partial X} + V\frac{\partial \Omega}{\partial Y}\right) = \frac{1}{Re}\left(\frac{\partial^2 \Omega}{\partial X^2} + \frac{\partial^2 \Omega}{\partial Y^2}\right) + Ri\left(\frac{\partial \theta}{\partial X} + N\frac{\partial \Phi}{\partial X}\right) \tag{8}$$

$$\frac{\partial \theta}{\partial \tau} + \left(U\frac{\partial \theta}{\partial X} + V\frac{\partial \theta}{\partial Y}\right) = \frac{1}{PrRe}\left(\frac{\partial^2 \theta}{\partial X^2} + \frac{\partial^2 \theta}{\partial Y^2}\right) \tag{9}$$

$$\frac{\partial \Phi}{\partial \tau} + \left(U\frac{\partial \Phi}{\partial X} + V\frac{\partial \Phi}{\partial Y}\right) = \frac{1}{ScRe}\left(\frac{\partial^2 \Phi}{\partial X^2} + \frac{\partial^2 \Phi}{\partial Y^2}\right) \tag{10}$$

Where U and V are the dimensionless velocity components, Ω the dimensionless vorticity and Ψ the dimensionless stream function, dimensionalized following the Eq. 11.

$$U = \frac{u}{U_0};\quad V = \frac{v}{U_0};\quad \Omega = \frac{\omega H}{U_0};\quad \Psi = \frac{\psi}{HU_0} \tag{11}$$

In which u and v are the dimensional velocity components and ω and ψ the dimensional vorticity and stream function, respectively. The buoyant ratio number $N = G_{r,S}/G_{rT}$ in the Eq. 8 represents the ratio between buoyant forces due to solutal gradients and temperature gradients and $Ri = G_{rT}/Re^2$ is the Richardson number.

Since all cavity walls are impenetrable, boundary conditions can be expressed as $\boldsymbol{V}.\vec{n} = 0$ and except for the sliding wall we set the tangential velocity to zero $\boldsymbol{V}.s = 0$ (no sliding boundary). This boundary conditions leads, in the vorticity-stream function formulation, to:

$$\left.\begin{aligned} \Omega &= -\frac{\partial \Psi^2}{\partial X^2} \quad at \quad Y = 0 \; or \; 1 \; and \; 0 < X < 1 \\ \Omega &= -\frac{\partial \Psi}{\partial Y^2} \quad at \quad X = 0 \; or \; 1 \; and \; 0 \le Y \le 1 \end{aligned}\right\} \tag{12}$$

From impenetrability we have that all walls must have the same stream function value (set to 0). The side walls are adiabatic which implies that $\partial\theta/\partial x = 0$ and $\partial\Phi/\partial x = 0$, for the top and bottom wall we impose the values of both dimensionless temperature and mass, 0 and 1, respectively. In addition, all variables are set to zero at the initial time ($\tau = 0 \rightarrow \Omega = \Psi = \Phi = \theta = 0$).

3.2 Numerical model

In this work, we solved the Eq.'s 7-10 using a finite difference scheme in a regular mesh with n_x x n_y points. To solve the time evolution we used a fourth order five stage SSPRK algorithm developed by Ruuth and Spiteri (2002), using approach similar to Cardoso and Bicudo (2009). In this scheme a property can be advanced in time using the following the equation:

$$\Gamma_{i,j}^{n+1} = \Gamma_{i,j}^{n} + \Delta t\, L(\Gamma_{i,j}^{n}) \tag{13}$$

Where Γ can be the vorticity, temperature or mass, Δt is the time step, n is the time index and i, j the mesh indices. The time evolution is achieved using a five-stage procedure, presented below:

$$\left.\begin{aligned}
\Gamma^{(1)} &= \Gamma^{n} + \left(\frac{38}{97}\right)\Delta t\, L(\Gamma^{n}) \\
\Gamma^{(2)} &= \left(\frac{667}{1501}\right)\Gamma^{n} + \left(\frac{869}{1564}\right)\Gamma^{(1)} + \left(\frac{1852}{5027}\right)\Delta t\, L\left(\Gamma^{(1)}\right) \\
\Gamma^{(3)} &= \left(\frac{364}{587}\right)\Gamma^{n} + \left(\frac{223}{587}\right)\Gamma^{(2)} + \left(\frac{233}{925}\right)\Delta t\, L\left(\Gamma^{(2)}\right) \\
\Gamma^{(4)} &= \left(\frac{1087}{6104}\right)\Gamma^{n} + \left(\frac{5017}{6104}\right)\Gamma^{(3)} + \left(\frac{2375}{4358}\right)\Delta t\, L\left(\Gamma^{(3)}\right) \\
\Gamma^{n+1} &= \left(\frac{1831}{3540}\right)\Gamma^{(2)} + \left(\frac{412}{4289}\right)\Gamma^{(3)} + \left(\frac{227}{3564}\right)\Delta t\, L\left(\Gamma^{(3)}\right) + \left(\frac{739}{1911}\right)\Gamma^{(4)} + \left(\frac{544}{2407}\right)\Delta t\, L\left(\Gamma^{(4)}\right)
\end{aligned}\right\} \tag{14}$$

The value of $L\left(\Gamma_{i,j}^{n}\right)$ is calculated using a second order central finite difference algorithm and represents the sum of advection and diffusion terms (and buoyancy terms in the case of the vorticity equation), given for vorticity, temperature and mass by:

$$\begin{aligned}
L\left(\Omega_{i,j}^{n}\right) = &-\left(\frac{\Psi_{i+1,j}^{n} - \Psi_{i-1,j}^{n}}{2\Delta y}\right)\left(\frac{\Omega_{i,j+1}^{n} - \Omega_{i,j-1}^{n}}{2\Delta x}\right) + \left(\frac{\Psi_{i,j+1}^{n} - \Psi_{i,j-1}^{n}}{2\Delta x}\right)\left(\frac{\Omega_{i+1,j}^{n} - \Omega_{i-1,j}^{n}}{2\Delta y}\right) \\
&+ \left(\frac{1}{Re}\right)\left[\left(\frac{\Omega_{i,j+1}^{n} - 2\Omega_{i,j}^{n} + \Omega_{i,j-1}^{n}}{\Delta x^2}\right) + \left(\frac{\Omega_{i+1,j}^{n} - 2\Omega_{i,j}^{n} + \Omega_{i-1,j}^{n}}{\Delta y^2}\right)\right] \\
&+ Ri\left[\left(\frac{\theta_{i,j+1}^{n} - \theta_{i,j-1}^{n}}{2\Delta x}\right) + N\left(\frac{\Phi_{i,j+1}^{n} - \Phi_{i,j-1}^{n}}{2\Delta x}\right)\right]
\end{aligned} \tag{15}$$

$$\begin{aligned}
L\left(\theta_{i,j}^{n}\right) = &-\left(\frac{\Psi_{i+1,j}^{n} - \Psi_{i-1,j}^{n}}{2\Delta y}\right)\left(\frac{\theta_{i,j+1}^{n} - \theta_{i,j-1}^{n}}{2\Delta x}\right) + \left(\frac{\Psi_{i,j+1}^{n} - \Psi_{i,j-1}^{n}}{2\Delta x}\right)\left(\frac{\theta_{i+1,j}^{n} - \theta_{i-1,j}^{n}}{2\Delta y}\right) \\
&+ \left(\frac{1}{PrRe}\right)\left[\left(\frac{\theta_{i,j+1}^{n} - 2\theta_{i,j}^{n} + \theta_{i,j-1}^{n}}{\Delta x^2}\right) + \left(\frac{\theta_{i+1,j}^{n} - 2\theta_{i,j}^{n} + \theta_{i-1,j}^{n}}{\Delta y^2}\right)\right]
\end{aligned} \tag{16}$$

$$\begin{aligned}
L\left(\Phi_{i,j}^{n}\right) = &-\left(\frac{\Psi_{i+1,j}^{n} - \Psi_{i-1,j}^{n}}{2\Delta y}\right)\left(\frac{\Phi_{i,j+1}^{n} - \Phi_{i,j-1}^{n}}{2\Delta x}\right) + \left(\frac{\Psi_{i,j+1}^{n} - \Psi_{i,j-1}^{n}}{2\Delta x}\right)\left(\frac{\Phi_{i+1,j}^{n} - \Phi_{i-1,j}^{n}}{2\Delta y}\right) \\
&+ \left(\frac{1}{ScRe}\right)\left[\left(\frac{\Phi_{i,j+1}^{n} - 2\Phi_{i,j}^{n} + \Phi_{i,j-1}^{n}}{\Delta x^2}\right) + \left(\frac{\Phi_{i+1,j}^{n} - 2\Phi_{i,j}^{n} + \Phi_{i-1,j}^{n}}{\Delta y^2}\right)\right]
\end{aligned} \tag{17}$$

Stream function is solved by the Poisson equation (Eq. 7) in the whole domain using a fourth order Sucessive Over Relaxation method (SOR). In this method the available estimates from other locations ($\Psi_{i+1,j}^{k+1}$) are used when they become available and use the current positions ($\Psi_{i,j}^{k}$) to improve the estimate $\Psi_{i,j}^{k+1}$. The fourth order SOR method is given by:

$$\Psi_{i,j}^{k+1} = \frac{3}{5}\frac{\beta}{a}(A + B + C) + (1 - \beta)\Psi_{i,j}^{k} \tag{18}$$

Where β is the relaxation parameter, k the interaction index and A, B and C are defined as:

$$\left.\begin{aligned} A &= b\left(\Psi_{i+1,j}^{k} + \Psi_{i-1,j}^{k+1}\right) + c\left(\Psi_{i,j+1}^{k} + \Psi_{i,j-1}^{k+1}\right) \\ B &= \frac{1}{12}\left(\Omega_{i+1,j}^{n} + \Omega_{i,j+1}^{n} + 8\Omega_{i,j}^{n} + \Omega_{i-1,j}^{n} + \Omega_{i,j-1}^{n}\right) \\ C &= \frac{1}{12}a\left(\Psi_{i+1,j+1}^{k} - 2\Psi_{i,j+1}^{k} + \Psi_{i-1,j+1}^{k+1} - 2\Psi_{i+1,j}^{k} - 2\Psi_{i-1,j}^{k+1} + \Psi_{i+1,j-1}^{k} - 2\Psi_{i,j+1}^{k} + \Psi_{i-1,j-1}^{k+1}\right) \end{aligned}\right\} \quad (19)$$

In which $a = b + c$, $b = 1/\Delta x^2$ and $c = 1/\Delta y^2$. The SOR algorithm iterates until the maximum absolute error measured between two successive iterations is lower than $\epsilon = 10^{-6}$.

At the boundaries, we applied the Thom's boundary condition for vorticity given by the following equation:

$$\left.\begin{aligned} \Omega_{ny,j} &= -2\frac{\Psi_{ny-1,j}}{\Delta y^2} - \frac{2\,U_o}{\Delta y} \quad at\ top\ wall\ (sliding\ wall) \\ \Omega_{1,j} &= -2\frac{\Psi_{2,j}}{\Delta y^2} \qquad at\ bottom\ wall \\ \Omega_{i,1} &= -2\frac{\Psi_{i,2}}{\Delta x^2} \qquad at\ left\ wall \\ \Omega_{i,nx} &= -2\frac{\Psi_{i,nx-1}}{\Delta x^2} \qquad at\ right\ wall \end{aligned}\right\} \quad (20)$$

Values of dimensionless temperature and mass were imposed at the top and bottom walls, 0 and 1, respectively. In the other walls, the boundary condition is defined as:

$$\left.\begin{aligned} \theta_{i,1} &= \theta_{i,2}\,, \quad \theta_{i,nx} = \theta_{i,nx-1} \\ \Phi_{i,1} &= \Phi_{i,2}, \quad \Phi_{i,nx} = \Phi_{i,nx-1} \end{aligned}\right\} \quad (21)$$

We considered three experiments to verify the effect of buoyancy ratio (N), Richardson number (Ri) and Lewis number (Le) on the steady state of vorticity, stream function, mass and temperature. In all experiment we considered $Re = 100$. Buoyancy ratio varies from -100 to 50, with $Ri = 0.01$ and $Le = 1$; Richardson number range from 10^{-3} to 10^{-1}, keeping $N = 1$ and $Le = 1$, and finally we simulated the effect of Lewis number from 5 to 25, with $N = 1$ and $Ri = 0.01$. Models runs until reach the steady state, in which the maximum absolute error of vorticity measured between two successive iterations is lower than $\epsilon = 10^{-6}$. The time step is chosen in function of the Reynolds number, following the relation:

$$\Delta t \leq \frac{1}{2}Re\left[\frac{1}{\left(\frac{1}{\Delta x^2}\right) + \left(\frac{1}{\Delta y^2}\right)}\right] \quad (22)$$

4. RESULTS AND DISCUSSION

4.1 Model Validation

The algorithm validation was carried out comparing the results of stream function and vorticity at center of the primary vortex with former studies for $Re = 1000$. Comparison is shown in Table 1. We also compared the profiles of velocities measured along the middle cross section of the cavity for $Re = 100$ and $Re = 400$. Comparison of present results and from Gia *et al.* (1982) are shown in Fig. 2. The results show good agreement with former works for Re up to 1000, comparing stream function, velocities and vorticity.

Table 1 - Comparison of the properties of the primary vortex; the maximum stream function, vorticity and the location of the vortex centre, for Re = 1000

Reference	Grid	Spatial accuracy	Ψ	Ω	x	y
Present work	81x81	Δh^2	**0.1165**	**1.9874**	**0.5375**	**0.5625**
Ertuk *et al*. (2005)	401x401	Δh^2	0.118585	2.062761	0.5300	0.5650
Botella & Peyret (1998)	160x160	Δh^2	0.1189366	2.067753	0.5308	0.5652
Schreiber &¨Keller (1986)	141x141	Δh^2	0.11603	2.0268	0.52857	0.56429
Wright & Gaskell (1995)	1024x1024	Δh^2	0.118821	2.06337	0.5308	0.5659
Li *et al*. (1995)	129x129	Δh^4	0.118448	2.05876	0.5313	0.5625
Ghia *et al.* (1982)	129x129	Δh^2	0.117929	2.04968	0.5313	0.5625
Gupta (1991)	41x41	Δh^4	0.111492	2.02763	0.525	0.575
Hou *et al*. (1995)	256x256	Δh^2	0.1178	2.0760	0.5333	0.5647

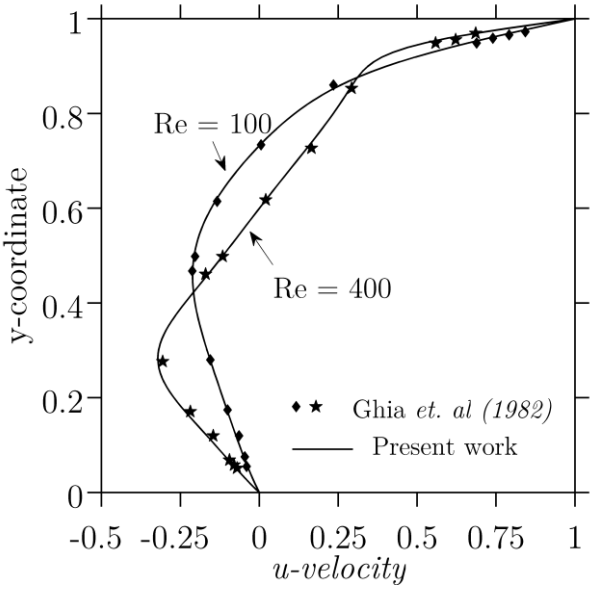

Figure 2 - Comparison of velocity profile in the middle cross section of the cavity and results from Ghia et al. (1982).

4.2 Effect of buoyant ratio (N)

We studied the effect the buoyant ratio considering $Re = 100$, $Ri = 0.01$ and $Le = 1$ (where $Sc = 1$ and $Pr = 1$), for negative and positive values, ranging from -100 to 50. The steady state of dimensionless stream-function, vorticity and temperature for negative values of N are shown in Fig. 3. We found very close results to Al-Amiri et al. (2007), in this case negative values of buoyant ratio means an opposing flow condition. For the larger values N (e.g. -100 – Fig. 3.a-c) we find a high opposing flow (counterclockwise vorticity) weakening the main flow and generating a counterclockwise eddy in the left bottom corner that grown as buoyant ratio diminishes, as shown in Fig 3.a, Fig 3.d and Fig 3.g in which for $N = -100$ it fills almost half of the cavity, such find is similar to Al-Amiri et al. (2007). Due to two opposing vortex the heat and mass transfer occur mainly by conduction (Al-Amiri et al. (2007)) and decrease causing isolines of temperature (and also concentration) to become parallels with the increase of N, where the main process that affect heat and mass conduction is the mechanical effect of the sliding lid (as shown by Al-Amiri et al. (2007)).

By other hand, positive values of buoyant ratio (Fig. 3) enhances the magnitudes of the main flow, due to the addition of clockwise vorticity, in this case we found that with the increase in the values of N and consequently velocities, the main vortex grow and its core moves toward the center of the cavity (as seen in the Fig 4.a, Fig 4.b and Fig 4.c). It also enhances the energy and mass transport (Fig 4.c, f, i) since buoyancy forces generate rotation in the same direction of the sling lid.

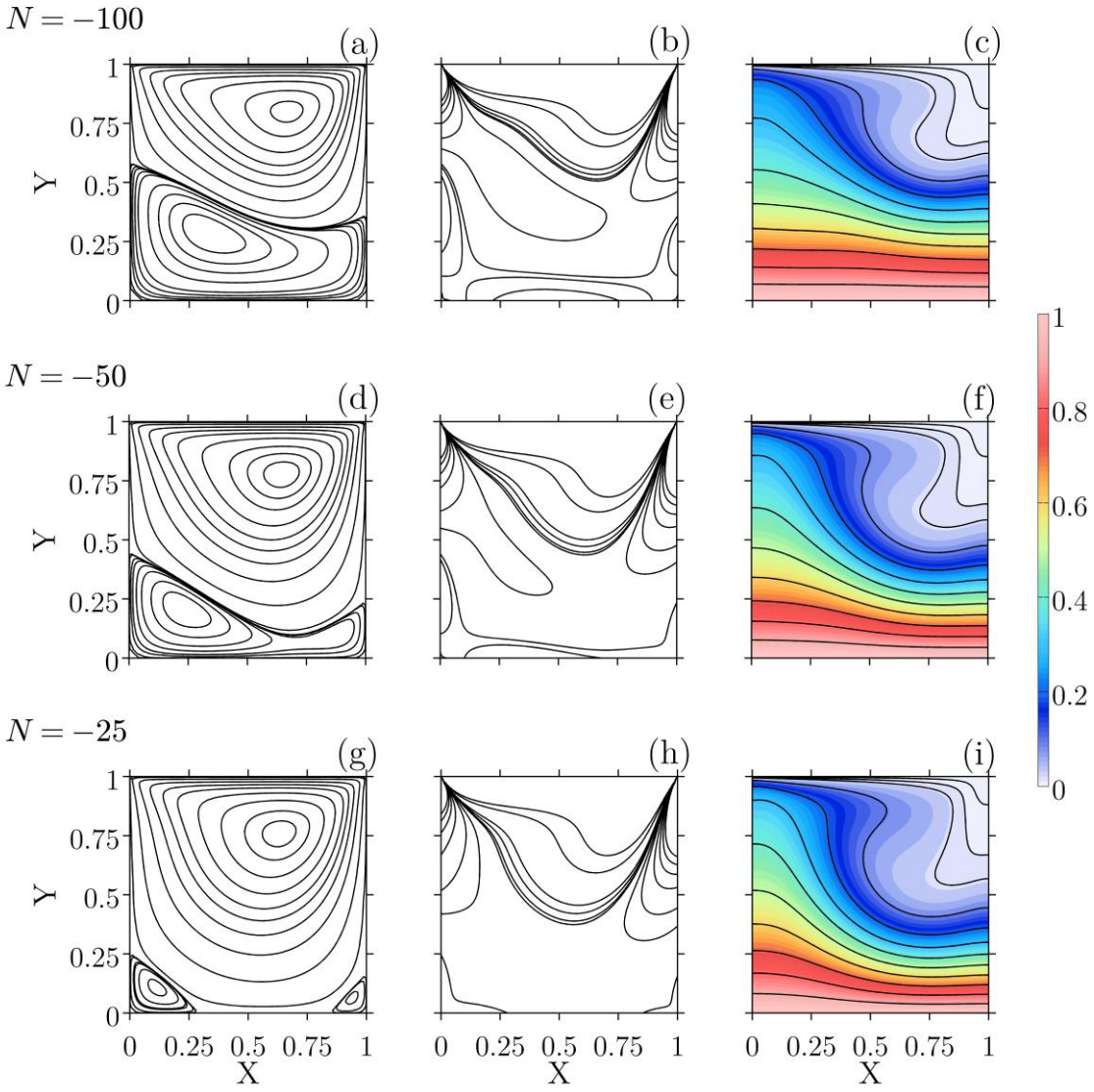

Figure 3 - Dimensionless stream-function (left column), vorticity (middle column) and temperature (right column) for negative buoyant ratio (N = −100 – first row, N = −50 – second row and N = −25 – third row).

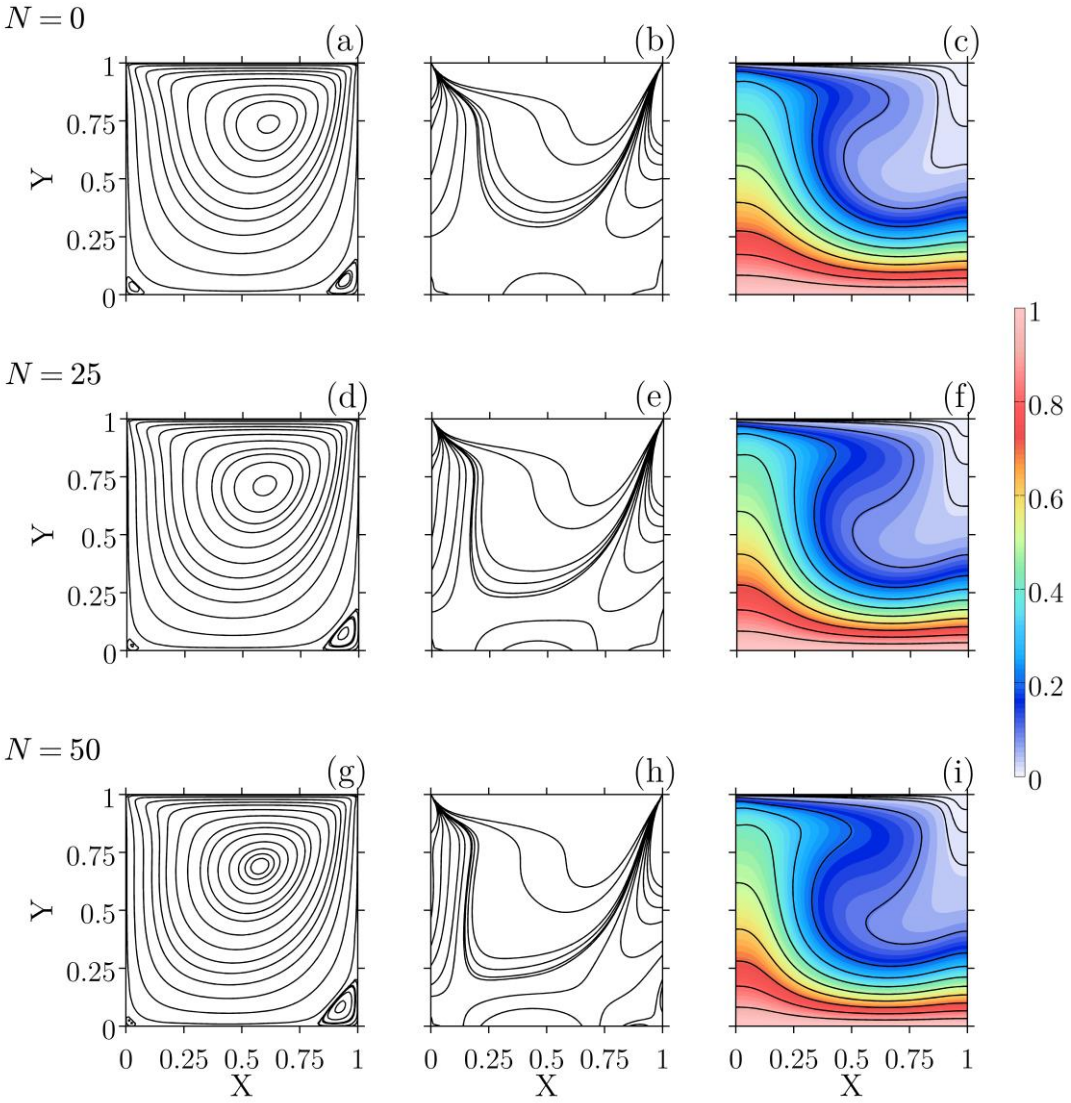

Figure 4 – Dimensionless stream-function (left column), vorticity (middle column) and temperature (right column) for negative buoyant ratio (N = 0 – first row, N = 25 – second row and N = 50 – third row).

4.3 Effect of Richardson number (Ri)

The effect of varying Richardson number on steady state streamline, vorticity and temperature is shown in the Fig. 5. We varied the Richardson number from 10^{-3} to 10^{-1} and set both Schmidt and Prandtl numbers to unity ($Sc = 1$ and $Pr = 1$). For $Ri < 10^{-1}$ the forced convection is main process in the mass and solutal transport and the overall flow remain quite the same, with a slight reduction of the flow intensity (as shown in Fig. 5.a-i). Also, a thinner boundary layer is formed with the decrease of the Richardson number. This can be attributed to the increase in the convection heat transfer mechanism, which causes steep temperature gradients in the vertical wall near to the bottom wall (Al-Amiri *et al.*, 2007). With the increase of Richardson number and consequently the convection, the convection of mass and temperature escalates the heat and mass transfer (as shown in Fig. 4. j-o). This leads to the formation of a counter-clock wise vortex in the bottom of the cavity occupying approximately half of the cavity (Fig. 4. m-o) for $Ri = 10^{1}$.

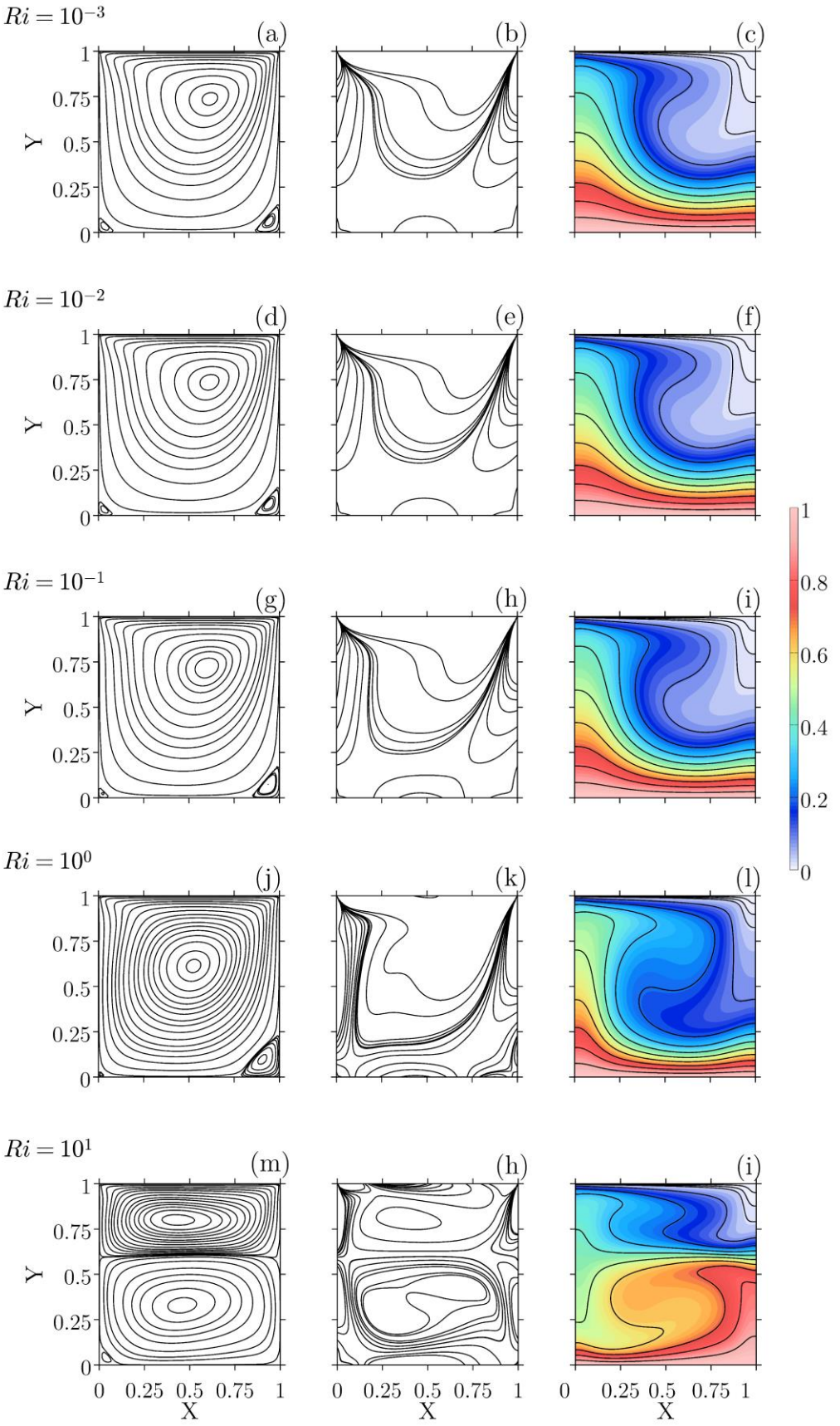

Figure 5 - Effect of varying Richardson number on streamline, vorticity and temperature considering $Le = 1$, $N = 1$ and $Re = 100$

4.3 Effect of Lewis Number (Le)

The effect of the varying Lewis number on streamlines, temperature and mass concentration is shown in Fig. 6. The Le number was varied between 5 and 50 (keeping $Pr = 1$ and varying the Schmidt number), while Ri was fixed at 0.01 and buoyant ratio to 1. The results show significant variations of mass concentration related to the depreciation in the diffusivity of mass concentration (as shown in Fig. 6. c, f, i). As presented by Al-Amiri *et al.* (2007), a thinner boundary layer forms along the bottom wall. Also, the result point out a minimal influence of Lewis number on isotherms and streamlines. This fact can be seen by means of the average dimensionless heat and mass flux (Nusselt – Nu and Sherwood - Sh numbers respectively), defined as:

$$\left.\begin{aligned} Nu &= \int_0^1 -\frac{\partial\theta}{\partial Y}\,dX \\ Sh &= \int_0^1 -\frac{\partial\Phi}{\partial Y}\,dX \end{aligned}\right\} \tag{23}$$

The average Nusselt number in function of buoyant ratio is shown in Fig. 7.a and average Nusselt and Sherwood numbers as function of Lewis number is shown in Fig. 7.b.

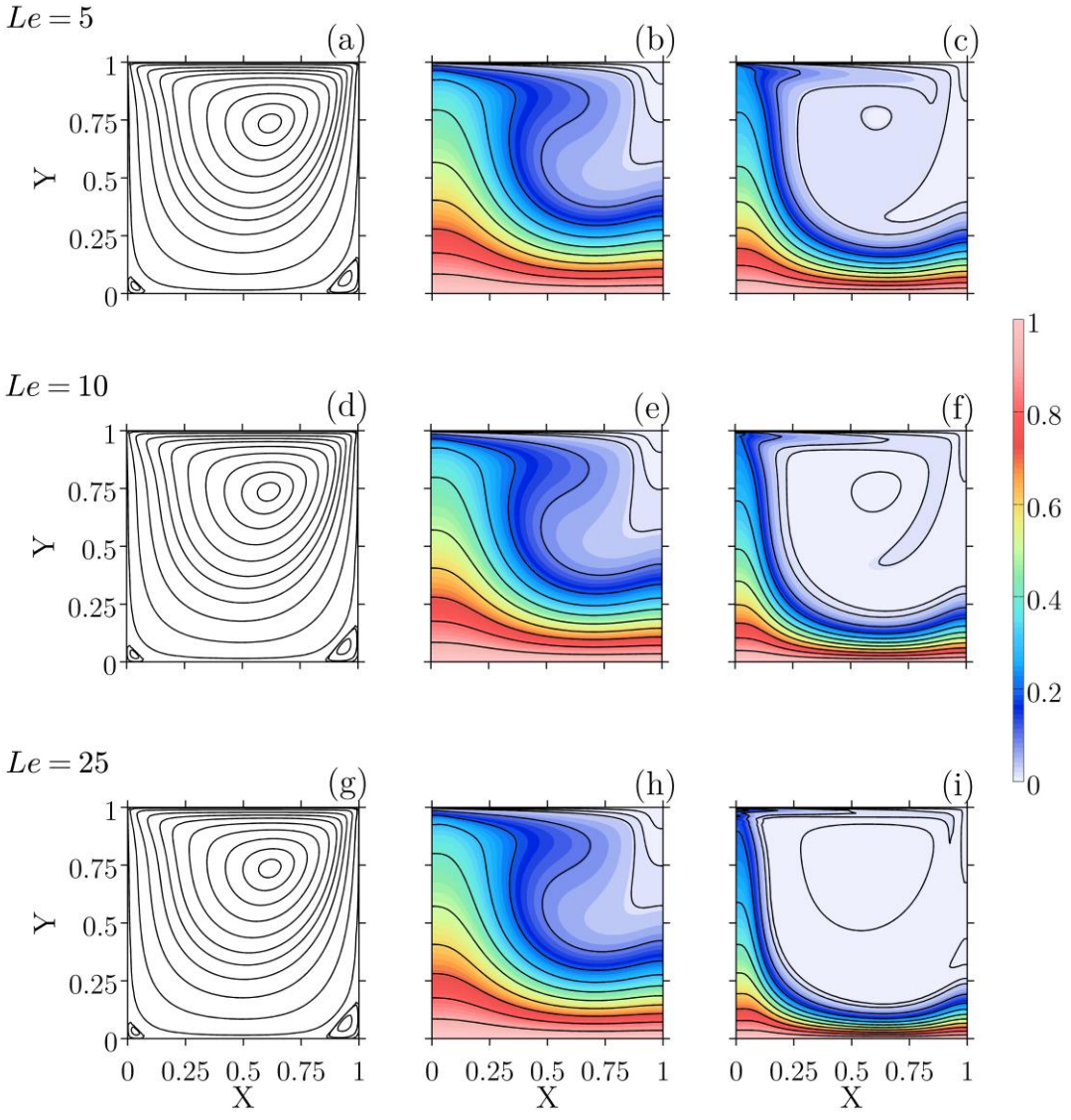

Figure 6 – Effect of varying Lewis number on streamlines (left column), temperature (middle column) and mass concentration (right column).

As shown in Fig 7.b, the Lewis number has a little influence on heat flux, while the mass flux (Sherwood number) has a rapid increase with the increase of Lewis number. In the other hand, the effect of the buoyant ratio on heat and mass flux is the same (Fig. 7.a) in which the flux is bigger for positive values of buoyant ratio.

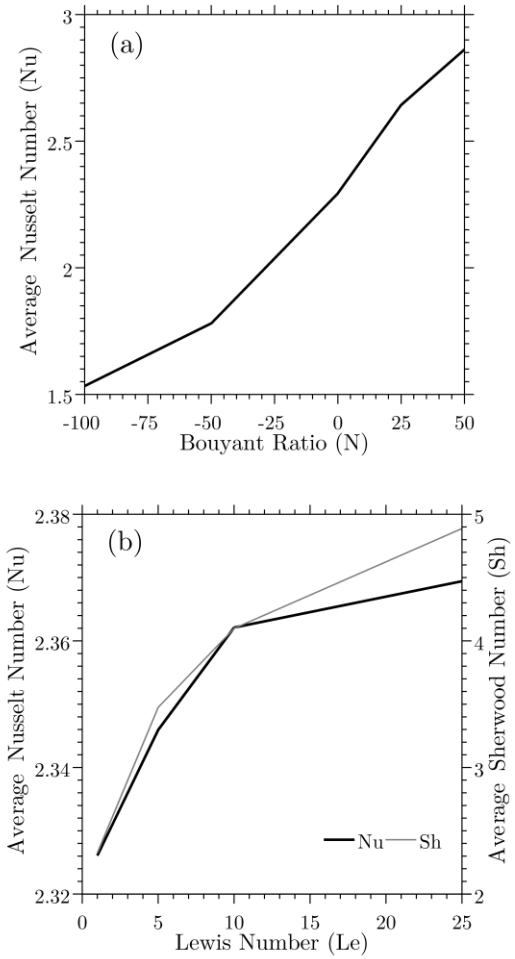

Figure 7 – Average Nusselt number as function of buoyant ratio (a) and Sherwood/Nusselt numbers as function of Lewis number (b).

5. CONCLUSIONS

In this work, we implement a second order finite difference numerical model to study hydrodynamics, mass and transport in a square lid-driven cavity. We analyzed the effect of buoyant ratio, Richardson and Lewis numbers on mass and heat transport. The results of the model showed good agreement with former studies and we find that negative values of buoyant ratio (opposing flow) leads to a generation of counter-clockwise vortex that increase in size as buoyant ratio decrease. By other hand positive values of buoyant ratio, enhances the fluid flow, moving the main vortex to the center of the cavity. We also found that convection is the main process for $Ri < 10^{-1}$.

5. REFERENCES

Al-Amiri, A., Khanafer, K., Bull, J., Pop, I. 2007. "Numerical simulation of combined thermal and mass transport in a square lid-driven cavity". International Journal of Heat and Mass Transfer. Vol. 46. pp. 662-671.

Botella, O., Peyret, R. 1998. Benchmark spectral results on the lid-driven cavity flow. Computers & Fluids. Vol. 27(4). pp. 421-433.

Bruneau, C., Saad, M. 2006. "The 2D lid-driven cavity problem revisited". Computers & Fluids. Vol. 35(3). pp. 326-348.

Cardoso, N., Bicudo, P. 2009. "Time dependent simuation of the driven lid cavity at high Reynolds number". Physics of Fluids. Vol. 1. pp. 1-20.

Erturk, E., Corke, T. C., Gökçöl, C. 2005. "Numerical solutions of 2-D steady incompressible driven cavity flow at high Reynolds numbers". International Journal for Numerical Methods in Fluids Int. Journal of Numerical Methods in Fluids. Vol. 48(7). Pp. 747-774.

Ghia U., Ghia K.N., Shin C.T. 1982. "High-resolutions for incompressible flows using Navier–Stokes equations and a multigrid method". Journal of Computer Physics. Vol. 48. pp. 313-352.

Gupta, M. M. 1991. "High accuracy solutions of incompressible Navier–Stokes equations". Journal of Computational Physics 1991. Vol. 9, pp. 343–359.

Hou, S., Zou, Q., Chen, S., Doolen, G., Cogley, A. C. 1995. "Simulation of cavity flow by the lattice Boltzmann method". Journal of Computational Physics. Vol. 118, pp. 329–347.

Li M., Tang, T., Fornberg, B. 1995. "A compact fourth-order finite difference scheme for the steady incompressible Navier–Stokes equations". International Journal for Numerical Methods in Fluids. Vol. 20, pp., 1137–1151.

Schreiber R and Keller, H.B. 1983. "Driven cavity fows by effcient numerical techniques". Journal of Computational Physics. Vol. 49, pp. 310–333.

Simonson, C.J. and Besant, R.W., 1999b. "Energy wheel effectiveness – part II: Correlations". International Journal of Heat and Mass Transfer, Vol. 42, pp. 2171–2185.

Spiteri, R. J., Ruuth, S. J. 2002. "A new class of optimal high-order strong-stability preserving time discretization methods". SIAM Journal of Numerical Anal. Vol. 40, pp. 469-491.

Tuckerman, D.B. and Pease, R.F.W., 2011. "Microchannel heat transfer: early history, commercial applications, and emerging opportunities". In Proceedings of the ASME 2011 9th International Conference on Nanochannels, Microchannels, and Minichannels. Edmonton, Alberta, Canada. Paper no. 58308.

Vajjha, R.S. and Das, D.K., 2009. "Experimental determination of thermal conductivity of three nanofluids and development of new correlations". International Journal of Heat and Mass Transfer, Vol. 52, No. 21-22, pp. 4675–4682.

Wright, N. G., Gaskell, P. H. 1995. "An effcient multigrid approach to solving highly recirculating fows". Computers and Fluids. Vol. 24, pp. 63–79.